

1 **High fidelity lineage tracing in mouse pre-implantation embryos**
2 **using primed conversion of photoconvertible proteins**

3 **Maaïke Welling^{1,†}, Manuel Alexander Mohr^{1,2,†}, Aaron Ponti¹, Lluc Rullan Sabater^{1,3},**
4 **Andrea Boni^{4,5}, Prisca Liberali⁴, Pawel Pelczar⁶, Periklis Pantazis^{1*}**

5 ¹Department for Biosystems Science and Engineering (D-BSSE), Eidgenössische Technische
6 Hochschule (ETH) Zurich, 4058 Basel, Switzerland

7 ²Howard Hughes Medical Institute, Janelia Research Campus, Ashburn, VA 20147, USA

8 ³present address: QuintilesIMS, 4053 Basel, Switzerland

9 ⁴Friedrich Miescher Institute for Biomedical Research (FMI), 4058 Basel, Switzerland

10 ⁵present address: Ecole polytechnique federale de Lausanne (EPFL), 1015 Lausanne,
11 Switzerland

12 ⁶Center for Transgenic Models (CTM), University of Basel, 4002 Basel, Switzerland

13 †Authors contributed equally to the work.

14 *Correspondence to: Periklis Pantazis, periklis.pantazis@bsse.ethz.ch

15 **Abstract**

16 Accurate lineage reconstruction of mammalian pre-implantation development is essential
17 for inferring the earliest cell fate decisions of mammalian development. Lineage tracing using
18 global labeling techniques is complicated by increasing cell density and rapid embryo rotation,
19 impeding automatic alignment and rendering accurate cell tracking of obtained four-dimensional
20 imaging data sets highly challenging. Here, we exploit the advantageous properties of primed
21 convertible fluorescent proteins (pr-pcFPs) to simultaneously visualize the global green and the
22 photoconverted red population to minimize tracking uncertainties over prolonged time windows.
23 Confined primed conversion of H2B-pr-mEosFP labeled nuclei combined with light-sheet
24 imaging greatly facilitates segmentation, classification, and tracking of individual nuclei from
25 the 4-cell stage up to the blastocyst. Using green and red labels as fiducial markers, we
26 computationally correct for rotational and translational drift and accomplish high fidelity lineage
27 tracing combined with a reduced data size – addressing majors concerns in the field of
28 volumetric embryo imaging.

29 **Introduction**

30 Accurate lineage tracing and precise tracking of single cells in pre-implantation embryos
31 is essential for a mechanistic understanding of the first cell fate decisions during mammalian
32 development¹. Selective plane illumination microscopy (SPIM) has the potential to play a major
33 role in achieving comprehensive, non-invasive imaging of mammalian pre-implantation
34 development. During these early steps of development, a major fraction of embryos (n=5/11,
35 45% in this study) exhibit confounding rotational and translational drift (Videos 1 and 2), which
36 often leads researchers to exclude these embryos from analysis, drastically decreasing efficiency,
37 losing valuable data, and potentially biasing downstream results^{2,3}. While high imaging rates
38 have helped to overcome these challenges for samples like zebrafish embryos, they demand
39 increased data storage capacities. Higher framerates can further increase photodamage from laser
40 overexposure and are hence less applicable for highly sensitive mouse embryos^{2,4}.

41 Sparse labeling strategies using green-to-red photoconvertible fluorescent proteins
42 (pcFPs) merit a great potential for facilitating lineage tracing and trophoctoderm (TE) and inner-
43 cell-mass (ICM) fate assignments after photoconversion⁵. However, to our knowledge these
44 sparse labels have not been combined with SPIM - presumably because photoconversion has
45 been limited by the need for axially unconfined, potentially photodamaging, intense violet light⁶.
46 Our recent report of a novel photochemical mechanism called “primed conversion” overcomes
47 this long-standing problem by using dual-wavelength illumination with blue 488nm, and far-red
48 730nm laser light instead. Importantly, primed conversion allows for confined conversion of
49 small volumes in three dimensions (3D) by selectively intersecting the two laser beams in a
50 common focal spot, yielding axial confinement unachievable using 405nm photoconversion^{7,8}.
51 While primed conversion was previously only reported for Dendra2, the discovery of the

52 mechanism responsible for primed conversion enabled the rational engineering of primed
53 convertible (“pr-”) variants of most pcFPs⁹. Consequently, we found that pr-pcFP variants based
54 on the Eos-family of *Anthozoa*-derived pcFPs undergo primed conversion efficiently and exhibit
55 high levels of brightness and photostability, essential properties for long-term imaging in a
56 SPIM⁹.

57 Here we show that primed conversion of single cells in early stages of mouse
58 development allows for computational correction of spatial and rotational drift, which minimizes
59 tracking and lineage tracing uncertainties over prolonged time windows.

60 **Results and Discussion**

61 **H2B-pr-mEosFP labeled cells primed converted at the 4-cell stage can be visualized up to** 62 **the blastocyst stage**

63 In order to assess which protein of the Eos-family is most suitable for long-term cell
64 tracking and lineage tracing experiments in mouse embryos, we directly compared pr-mEos2 and
65 pr-mEosFP. We injected mouse zygotes with mRNAs encoding for the histone fusions H2B-pr-
66 mEos2 or H2B-pr-mEosFP and imaged them at different developmental stages to observe
67 potential detrimental effects. Embryos injected with mRNA encoding for H2B-pr-mEosFP
68 showed no visible signs of developmental impairment, similar to un-injected control embryos
69 (Figure 1 – figure supplement 1a). In contrast, H2B-pr-mEos2 injected embryos showed partly
70 divided, seemingly connected nuclei and prematurely arrested in development (n=30/30) (Figure
71 1 – figure supplement 1b). This apparent inability to separate the nuclei during cell division is
72 likely due to a residual tendency of mEos2 to oligomerize, as proposed previously¹⁰ (Figure 1 –
73 figure supplement 1). As a consequence, we identified primed convertible mEosFP (pr-mEosFP)

74 as the optimal fluorescent protein variant for *in vivo* primed conversion followed by long-term
75 imaging.

76 Next, we investigated whether a single round of green-to-red photoconversion at the 4-
77 cell stage would create a sufficiently large pool of red-converted protein that could be followed
78 throughout development until the early blastocyst stage. For this purpose, we used confined
79 primed conversion to photoconvert a single nucleus of an H2B-pr-mEosFP expressing embryo at
80 the 4-cell stage⁸, and monitored early embryo development for 60 hours in an inverted SPIM²
81 (Figure 1a). Photoconverted embryos developed healthily and the red daughter cells of the
82 initially primed converted single cell were clearly distinguishable from their non-converted green
83 counterparts up to the blastocyst stage (Figure 1b; Figure 1 – supplement 2).

84 **Dual labeling of pre-implantation embryos greatly facilitates automatic** 85 **segmentation, tracking and lineage tracing**

86 The observation that cells converted at the 4-cell stage can be visualized up to the
87 blastocyst stage prompted us to ask if sparsely labeled subsets of cells could aid computational
88 reorientation and automated lineage tracing in embryos that exhibit dramatic rotational and
89 translational drift, (Videos 1 and 2). To this end, we developed a computational pipeline for
90 automated segmentation, cell tracking, and lineage tracing. This algorithm uniquely takes
91 advantage of the sparse red population to correct for translational and rotational drift as well as to
92 simplify lineage reconstruction (Figure 2a). In the 5-dimensional (5D, i.e. 3 spatial dimensions,
93 time, color) imaging data, cells were first segmented based on size, shape, and fluorescence
94 taking into account both color channels. Specifically, as the red signal diminishes over time
95 while red background autofluorescence increases, the dual labeling enables the identification of
96 weaker fluorescent red nuclei at late time points by their overlap with green signal that has lower

97 autofluorescence (Figure 2a, left column). Also, the dual color information allows for cell
98 distinction in instances otherwise rendered ambiguous through high cell density and proximity of
99 nuclei. For instance, we were able to distinguish nuclei that would have been identified as a
100 single nucleus even after manual validation (Figure 2 – figure supplement 1a-c).

101 In a second step, the embryo was centered at its fluorescence center of mass, cropped and
102 rotated, such that the red center of mass was oriented to the same side of the embryo in every
103 time frame to compensate for rotational and translational drift (Figure 2a, middle column; Video
104 3 and 4). The resulting high-quality 5D cropped and registered datasets were on average $61 \pm 12\%$
105 smaller in size (Figure 2 – figure supplement 2). The automatic tracing of a realigned embryo
106 resulted in greatly improved lineage tracing fidelity compared to a naïve state-of-the-art lineage-
107 tracing algorithm that was not able to reconstruct a lineage tree from rotating and spatially
108 drifting embryos imaged with a time interval of 15 or 7.5 minutes (Bitplane Imaris cell lineage
109 package) (Figure 2b; Figure 2 – figure supplement 3). Separating the green and red channels to
110 generate two less complex datasets during lineage reconstruction further increased the fidelity of
111 lineage tracing versus the dataset consisting of the green channel alone (Figure 2a, right column;
112 Figure 2 – figure supplement 3). We assessed the power of our newly created lineage tracing
113 algorithm by comparing the lineage trees obtained i) without corrections, ii) after embryo
114 realignment with all algorithmic corrections, and iii) after final manual review by calculating the
115 total distance between these lineage trees (see methods for more details)¹¹. Notably, the resulting
116 lineage trees required a minimal amount of time for manual corrections (i.e. 1-1.5 hours for the
117 total lineage tree).

118 **Summary and conclusion**

119 In summary, the presented approach enables fast, automated, high fidelity lineage tracing
120 of mammalian pre-implantation development combined with reduced illumination time and data
121 volume, key considerations for handling and analyzing data by the biological community¹². In
122 addition, the ability to correct for both spatial and rotational drift overcomes the need to exclude
123 spinning embryos from the analysis. On a different note, it might enable the experimenter to
124 achieve similar tracing quality with datasets acquired at lower sampling rate. In the future,
125 implementing primed conversion to take place inside the SPIM used for volumetric imaging, will
126 allow for repeated manual or automatic primed conversion of nuclei once the red fluorescence
127 drops below a user-defined threshold. Similar pulse-chase experiments can then be extended
128 even longer, ultimately being only limited by the rate of new green pr-pcFP synthesis. The
129 combination of confined primed conversion of pr-pcFPs with our imaging pipeline will allow
130 researchers to get more accurate insight into the dynamic processes responsible for cell fate
131 decisions in the early mammalian embryo.

132

133 **Materials and Methods**

134 **Molecular cloning and mRNA preparation**

135 The coding sequences for pr-mEosFP and pCS2+-H2B-pr-EosFP were obtained by PCR
136 amplification from pQE32-pr-mEosFP (Addgene No. 99213) and pRSET-pr-mEos2 (gift from
137 Dominique Bourgeois) and cloned into pCS2+-H2B-Dendra2 using AgeI and SnaBI, hence
138 replacing the Dendra2 coding sequence to obtain pCS2+-H2B-pr-EosFP (Addgene No.:
139 XXXXX) and pCS2+-H2B-pr-Eos2. mRNA was synthesized using the mMESSAGING
140 mMACHINE kit (ThermoFisher Scientific), followed by poly-A-tailing (ThermoFisher
141 Scientific), and purified using a Qiagen RNeasy kit according to manufacturer guidelines.

142 **mRNA microinjection of mouse preimplantation embryos and ex utero culture up to 4-cell**
143 **stage**

144 C57/Bl6 wild-type females were superovulated by hormone priming, mated to C57/Bl6
145 males, and mated females were euthanized by CO₂ asphyxiation. Embryos were recovered by
146 flushing oviducts as described previously^{8,13}. Embryos were cultured at 37°C and 5% CO₂ in
147 KSOM+AA medium covered with mineral oil. mRNA constructs were microinjected into the
148 pro-nucleus at 50 ng/ul or in both cells in two-cell stage embryos, following standard protocols.
149 All these experiments were approved by the veterinary authority of the canton Basel Stadt,
150 Swizerland.

151 **Confined primed conversion of single nuclei in mouse embryos**

152 Confined primed conversion of single nuclei was performed on mouse embryos at the 4-
153 cell stage as previously described in great detail⁸.

154 **Volumetric imaging of mouse pre-implantation embryos**

155 Right after confined primed conversion was performed, the 4-cell stage embryos were
156 transferred to a pre-equilibrated, inverted SPIM setup and continuously cultured/imaged until
157 they reached blastocyst stage². For each embryo a z-stack consisting of 80 planes, 3 µm apart,
158 was acquired every 7.5 or 15 minutes.

159 **Mouse embryo lineage tracing**

160 To establish a reference, mouse embryos were lineage traced using the state-of-the-art
161 Imaris lineage tracing package (Bitplane, CH). The automated high-fidelity mouse embryo drift
162 correction and lineage-tracing algorithm described here is explained in detail below.

163 **Detailed description of the automatic segmentation, registration, and lineage tracing**
164 **algorithm**

165 5D movies of photoconverted mouse embryos were processed with the following pipeline
166 using a custom MATLAB code implemented in Imaris (Bitplane, CH).

167 Cell Segmentation:

168 1. Detect green and red cells using the Spot detector in Imaris. Use low threshold to
169 segment all cells even at the cost of including spurious spots. Allow spot radius to be
170 adapted to more accurately fit the volume of the segmented cell. Bright but very small
171 spots can easily be filtered out during segmentation.

172 First validation

173 2. Use the green spot positions to estimate the embryo diameter and discard green spots that
174 are likely to be outside of the embryo. The radius of the embryo is roughly estimated as
175 the median of all maximal inter-spot distances. A user-defined multiplicative factor can
176 optionally compensate for estimation errors and prevent cells at the boundary of the
177 embryo to be discarded should this constraint be too stringent.

178 3. Search for spots that occur within a small defined distance from a spot in the same
179 channel, discard all wrongly segmented double spots on one nucleus and replace them by
180 one new spot.

181 4. Discard all spurious red spots that do not colocalize with a green spot. Note that due to
182 the equilibrium between protonated and de-protonated chromophore, green to red
183 photoconversion of pcFPs is never exhaustive and will always retain a green population,
184 rendering this quality control step possible.

185 5. A red spot discarded during the first validation can optionally be recovered if there is a
186 valid red spot in previous time point within a user-defined search radius. This adjustment
187 compensates for remaining miss-segmentations in the green channel.

188 Embryo alignment (drift and rotational correction)/Cropping:

189 6. Imaris Reference Frame Objects are created in MATLAB for each time point: their origin
190 is set at the position of the center of mass (COM) of the green spots and their orientation
191 is given by the vector $\Delta\mathbf{COM} = \mathbf{COM}^{red} - \mathbf{COM}^{green}$. This correction still has one
192 degree of freedom. The rotation angle around the reference frame axis is obtained by
193 comparing the positions of the green spots at timepoints t and $t - 1$ over 360 1-degree
194 rotations and by choosing the angle that minimizes the cell drift between time points. The
195 resampling is performed in Imaris.

196 7. Crop data to the smallest bounding volume.

197 Second validation and subsetting

198 8. To pick up red cells that were not recovered previously, re-run the first validation on the
199 re-aligned embryo.

200 9. Create a new spot object that contains the subset of green cells that do not colocalize with
201 red cells.

202 Lineage tree reconstruction

203 10. Imaris' Lineage module is used to track the cells over time and reconstruct their lineage
204 tree. The subsetting in the previous step allows us to reduce the complexity of the lineage
205 tracing problem by breaking it down into two simpler, computationally less expansive,
206 disjoint problems.

207 **Comparative Analysis of lineage trees.**

208 To assess the power of our newly created algorithm, we sought to compare the lineage
209 trees obtained with i) no corrections, ii) after embryo realignment with all algorithmic
210 corrections, and iii) after final manual review. We quantified the effects of the corrections and
211 validations on the quality of the lineage trees by calculating the total distance between the
212 lineage trees using the implementation of the tree Zhang-Shasha edit distance algorithm¹¹ by Tim
213 Henderson and Steve Johnson¹⁴. The zss algorithm assigns a (user-defined) cost for each node
214 insertion, removal, and update necessary to transform an ordered tree into another, and gives
215 therefore a quantitative measure of dissimilarity of the two trees. Small tracking differences
216 between corrected and uncorrected trees, however, can result in quite large tree distances if the
217 zss algorithm is applied to the complete trees. A correction that relinks one cell to its mother cell
218 in just one time point causes the whole branch to be flagged as incorrect, and the longer the
219 branch, the higher the distance between the trees. In other words, the earlier the tracking error
220 occurs, the larger the distance; yet, only the first time point in the track is incorrect, and its
221 penalty should be the same whether it happens at the beginning of the time series or the end.

222 To circumvent these issues, we applied the algorithm to a condensed version of the
223 lineage trees. The condensed tree retains only the branch points of the original lineage tree (i.e.
224 the cell divisions). Also, each branch point stores information about the original number of child
225 nodes in its branches (i.e. the number of time points the daughter cells were tracked until their
226 next cell division). The distance between condensed trees will flag positions where cell divisions
227 were tracked incorrectly and tracks that have different lengths, without causing an explosion in
228 the reported distance.

229 Since our acquisitions started at the 4-cell stage, we aimed to build a tree for each of the
230 original four cells (one containing the progeny of the primed converted cell). The final, manually
231 curated lineage was used as ground truth to quantify the effects of the various algorithmic
232 correction steps. The sets of trees across correction schemes were assigned to each other by
233 minimizing the spatial and temporal distance of their origins. After condensation, their pairwise
234 distances were calculated. All distances were summed to give the total lineage tree difference. In
235 addition, spurious trees that resulted from bad segmentation and tracking were not used for the
236 distance calculation, since they already indirectly affected the difference of the tree from which
237 they were erroneously detached.

238

239 **Funding**

240 **Rubicon fellowship from the Netherlands Organisation for Scientific Research (NWO)**

241 - Maaïke Welling

242 **Howard Hughes Medical Institute Janelia graduate research fellowship**

243 - Manuel A Mohr

244 **Howard Hughes Medical Institute Janelia's Visiting Scientist Program**

245 - Periklis Pantazis

246 **Swiss National Science Foundation (SNF grant no. 31003A_144048)**

247 **European Union Seventh Framework Program (Marie Curie Career Integration Grant**
248 **(CIG) no. 334552)**

249 The funding sources had no role in the study design, data collection and interpretation, or the
250 decision to submit the work for publication.

251 **Acknowledgements:**

252
253 We thank all members of the Pantazis lab and especially M. Haffner for discussion and
254 advice. We thank U. Nienhaus and K. Nienhaus for discussions and advice as well as E.
255 Schreiter, and L. Looger for discussions; W.P. Dempsey for feedback on the manuscript and C.
256 Morkunas for administrative management.

257 **Competing interests**

258 P.Pa is an inventor on a patent application filed by ETH Zurich that describes primed
259 conversion. P.Pa. and M.A.M. are inventors on a provisional patent application filed by HHMI
260 and ETH Zurich that describes pr-mEosFP.

261 **Individual Author Contributions**

262 M.A.M., and P.Pa. conceived the idea. M.W. and M.A.M planned and M.W. carried out
263 imaging experiments with the help of M.A.M. and L.R.S. A.B. and P.L. assisted with design and
264 execution of inverted light-sheet imaging experiments and P.Pe. performed mouse embryo
265 injections. M.W., A.P. and M.A.M conceived and A.P. implemented the software with the help
266 of M.W. and M.A.M. M.W. and M.A.M. wrote the manuscript with the help of P.Pa. and A.P.
267 and editing input from the other authors. P.Pa. supervised the work.

268 **References:**

269 1. Welling, M., Ponti, A. & Pantazis, P. Symmetry breaking in the early mammalian embryo:
270 the case for quantitative single-cell imaging analysis. *Mol. Hum. Reprod.* **22**, 172–181
271 (2016).

- 272 2. Strnad, P. *et al.* Inverted light-sheet microscope for imaging mouse pre-implantation
273 development. *Nat. Methods* **13**, 139–142 (2016).
- 274 3. Motosugi, N., Bauer, T., Polanski, Z., Solter, D. & Hiiragi, T. Polarity of the mouse
275 embryo is established at blastocyst and is not prepatterned. *Genes Dev.* **19**, 1081–1092
276 (2005).
- 277 4. Takenaka, M., Horiuchi, T. & Yanagimachi, R. Effects of light on development of
278 mammalian zygotes. *Proc. Natl. Acad. Sci. U. S. A.* **104**, 14289–93 (2007).
- 279 5. Kurotaki, Y., Hatta, K., Nakao, K., Nabeshima, Y.-I. & Fujimori, T. Blastocyst axis is
280 specified independently of early cell lineage but aligns with the ZP shape. *Science* **316**,
281 719–723 (2007).
- 282 6. Post, J. N., Lidke, K. A., Rieger, B. & Arndt-Jovin, D. J. One- and two-photon
283 photoactivation of a paGFP-fusion protein in live *Drosophila* embryos. *FEBS Lett.* **579**,
284 325–30 (2005).
- 285 7. Dempsey, W. P. *et al.* In vivo single-cell labeling by confined primed conversion. *Nat.*
286 *Methods* **12**, 645–648 (2015).
- 287 8. Mohr, M. A., Argast, P. & Pantazis, P. Labeling cellular structures in vivo using confined
288 primed conversion of photoconvertible fluorescent proteins. *Nat. Protoc.* **11**, 2419–2431
289 (2016).
- 290 9. Mohr, M. A. *et al.* Rational Engineering of Photoconvertible Fluorescent Proteins for
291 Dual-Color Fluorescence Nanoscopy Enabled by a Triplet-State Mechanism of Primed
292 Conversion. *Angew. Chemie Int. Ed.* **56**, 11628–11633 (2017).
- 293 10. Zhang, M. *et al.* Rational design of true monomeric and bright photoactivatable

- 294 fluorescent proteins. *Nat. Methods* **9**, 727–729 (2012).
- 295 11. Zhang, K. & Shasha, D. Simple Fast Algorithms for the Editing Distance between Trees
296 and Related Problems. *SIAM J. Comput.* **18**, 1245–1262 (1989).
- 297 12. Pantazis, P. & Supatto, W. Advances in whole-embryo imaging: a quantitative transition
298 is underway. *Nat. Rev. Mol. Cell Biol.* **15**, 327–39 (2014).
- 299 13. Plachta, N., Bollenbach, T., Pease, S., Fraser, S. E. & Pantazis, P. Oct4 kinetics predict
300 cell lineage patterning in the early mammalian embryo. *Nat. Cell Biol.* **13**, 117–23 (2011).
- 301 14. Henderson, T. & Johnson, S. Tree edit distance using the Zhang Shasha algorithm. *v1.1.4*
302 (2013). at <<https://github.com/timtadh/zhang-shasha>>

303 **Figure legends**

304 **Figure 1. H2B-pr-mEosFP injected embryos develop to the blastocyst stage**

305 (a) Experimental setup: Zygotes are injected with H2B-pr-mEosFP mRNA. At the 4-cell stage
306 confined primed conversion of a single nucleus is performed using intersecting 488nm and
307 730nm lasers. The embryos are transferred to an inverted SPIM for non-invasive imaging of their
308 development up to the blastocyst stage. Images are taken every 7.5 or 15 minutes. (b) Embryos
309 injected with mRNA encoding H2B-pr-mEosFP and converted at the 4-cell-stage develop
310 normally and maintain visibility of the red label up to the early blastocyst stage. pr-mEosFP
311 fluorescence (green) and primed converted pr-mEosFP fluorescence (magenta). $N \geq 200$ out of \geq
312 10 independent experiments. Scale bar, 20 μm .

313

314 **Figure 2. An automated segmentation, tracking, and lineage tracing pipeline results in**
315 **efficient lineage reconstruction of embryos with high spatial and rotational drift**

316 **(a)** Overview of the pipeline used for reliable automated segmentation, tracking, and lineage
317 tracing of the imaged embryos; 1) Segmentation: low thresholds are used for the spot detection
318 in both the green and red channel to enable detection of dimmer cells at later developmental time
319 points. Incorrectly segmented spots are excluded by defined filters: i) exclusion of spots outside
320 of a defined radius of the embryo, ii) replacement of incorrectly segmented double spots by one
321 spot per one nucleus, and ii) exclusion of red spots that do not colocalize with green nuclear
322 spots. 2) Tracking: Spatial drift as well as rapid embryo rotation complicates tracking nuclei over
323 prolonged time windows. The segmented nuclei are used for defining reference frames based on
324 the center of mass of the green nuclei and the orientation of the red nuclei. The alignment of the
325 references frames of each time point compensates the spatial and rotational drifts. 3) Lineage
326 tracing: Automated lineage tree reconstruction can make false connections when cells are
327 dividing. By separating the calculation of the lineage trees in the photoconverted red channel
328 from the green channel, the less complex datasets for each channel result in more consistent
329 lineage tracing. pr-mEosFP fluorescence (green) and primed converted pr-mEosFP fluorescence
330 (magenta) overlaid with segmentation results (green and Magenta spheres); Scale bar, 20 μm **(b)**
331 Lineage trees from the same embryo (corresponding to Video 1 and 3) reconstructed from
332 segmented nuclei before correction for rotational and translational drift (left), after correction for
333 rotational and translational drift for the red channel (second left), after correction for rotational
334 and translational drift for the green channel minus the spots that colocalize with the red spots
335 (second right), and after final manual lineage reconstruction (right). The embryo was imaged
336 every 15 minutes.

337

338 **Video 1. Video of a developing embryo before drift correction.**

339 Timelapse video of an example embryo, which shows strong spatial and rotational drift before
340 drift correction. pr-mEosFP fluorescence (green) and primed converted pr-mEosFP fluorescence
341 (red). Scale bars, 15 μm ; framerate: one frame every 15 minutes.

342

343 **Video 2. Video of another developing embryo before drift correction.**

344 Timelapse video of an example embryo, which shows strong spatial and rotational drift before
345 drift correction. pr-mEosFP fluorescence (green) and primed converted pr-mEosFP fluorescence
346 (red). Scale bars, 10 μm ; framerate: one frame every 7.5 minutes.

347

348 **Video 3. Video of a developing embryo (same as in Video 1) after drift correction.**

349 Timelapse video of the example embryo from Video 1 after drift correction. pr-mEosFP
350 fluorescence (green) and primed converted pr-mEosFP fluorescence (red). Corresponding
351 lineage trees are displayed in Figure 2d. Scale bars, 15 μm ; framerate: one frame every
352 15 minutes.

353

354 **Video 4. Video of a developing embryo (same as in Video 2) after drift correction.**

355 Timelapse video of the example embryo from Video 2 after drift correction. pr-mEosFP
356 fluorescence (green) and primed converted pr-mEosFP fluorescence (red). Corresponding
357 lineage trees are displayed in Figure 2- figure supplement 3. Scale bars, 10 μm ; framerate: one
358 frame every 7.5 minutes.

359

360 **Supplementary files include:**

361

362 Figure 1 – figure supplement 1: Embryos expressing H2B-pr-mEosFP develop normally.

363 Figure 1 – figure supplement 2: Visualizing the lineage of a single cell up to the blastocyst stage
364 using primed converted at the 4-cell stage.

365 Figure 2 – figure supplement 1: Dual labeling facilitates segmentation in dense environments.

366 Figure 2 – figure supplement 2: Embryo dataset size before and after registration.

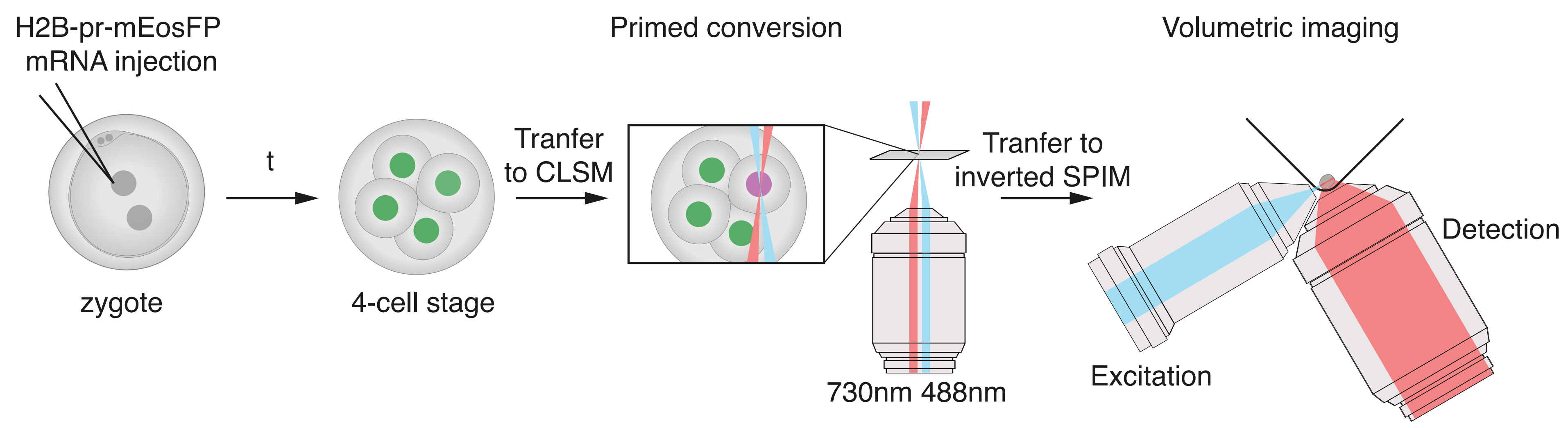
367 Figure 2 – figure supplement 3: Comparison of lineage tracing results.

368 Supplemental methods: Detailed description of the automatic segmentation, registration, and
369 lineage tracing algorithm

370

Figure 1

a



b

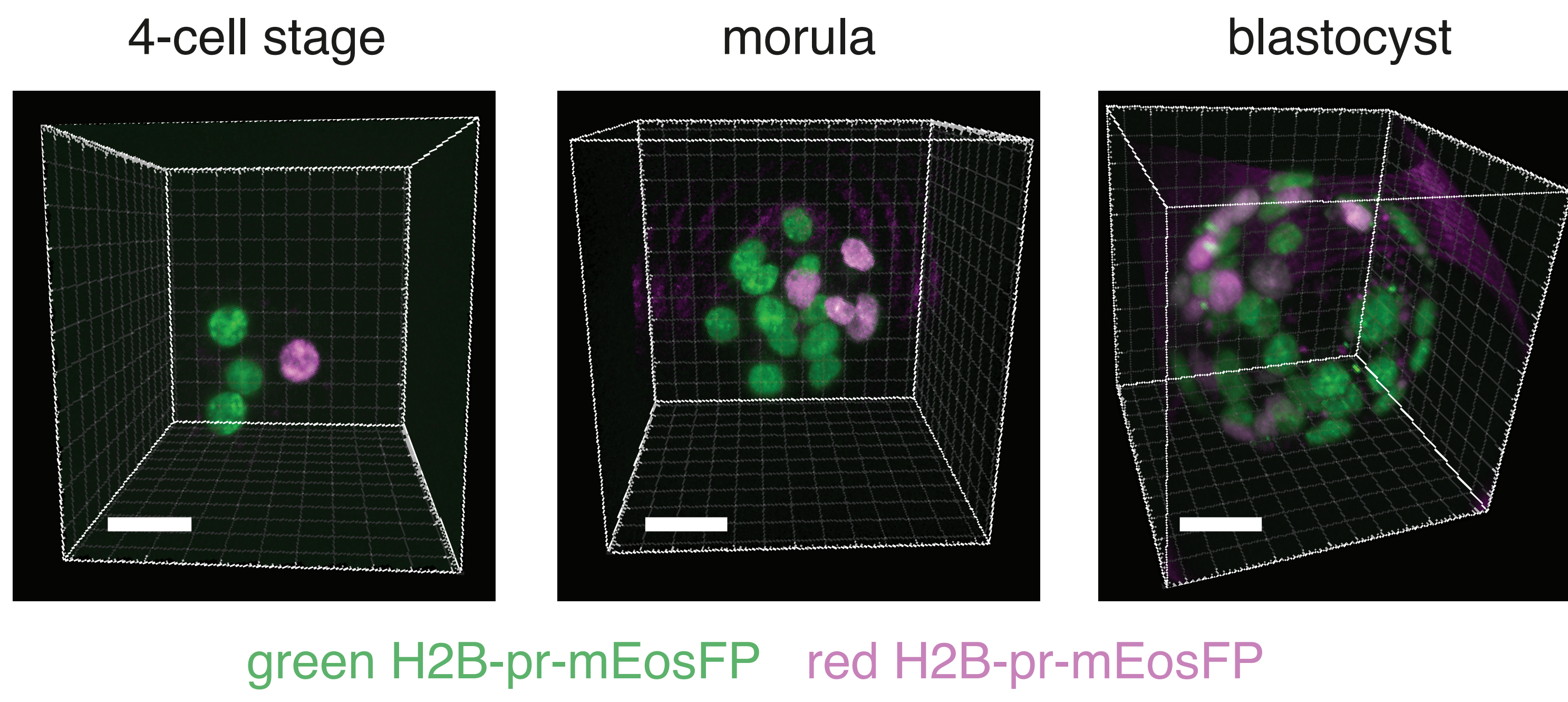
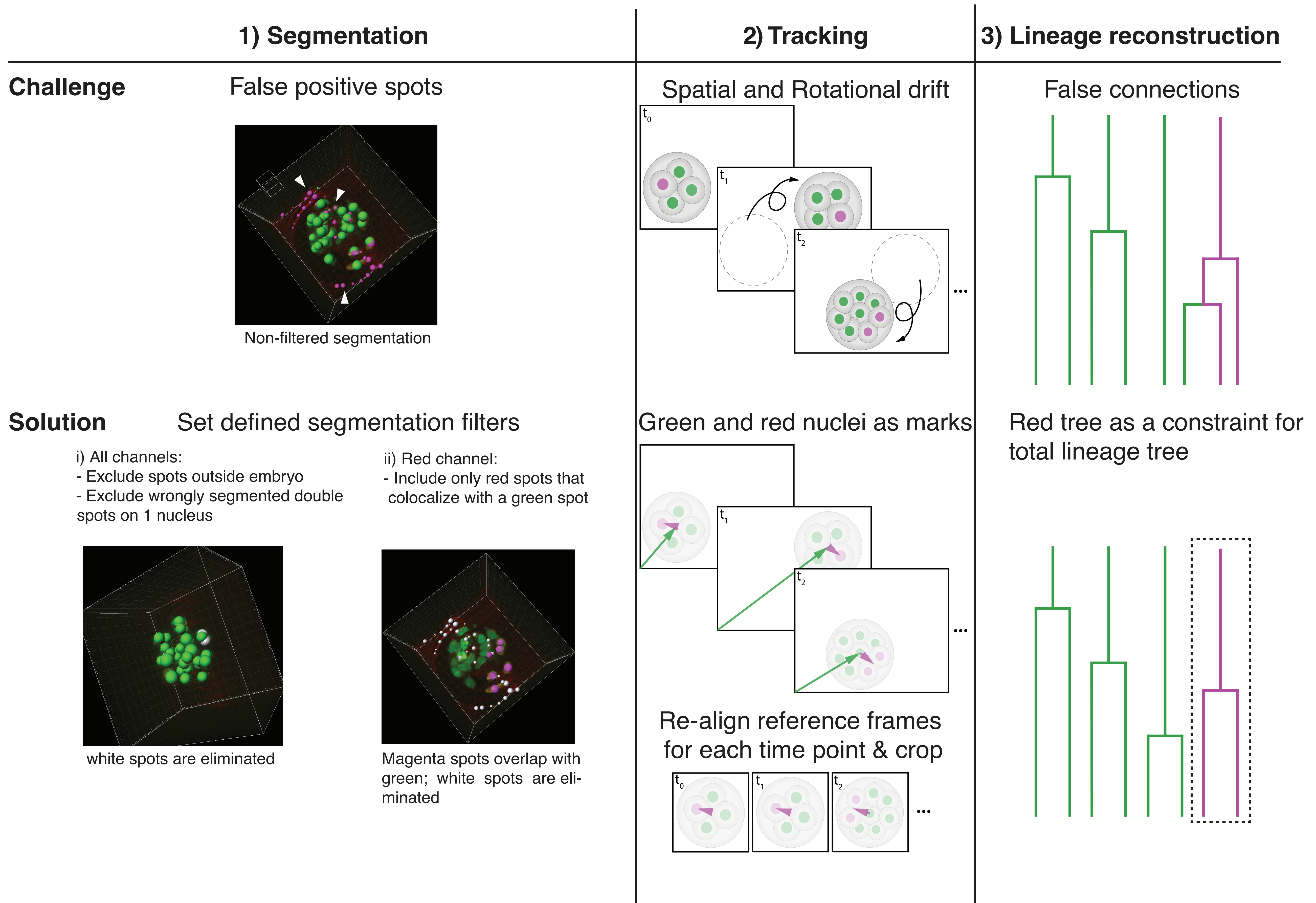


Figure 2

a



b

